

6-2018

Modifying the size of nanopores of alginate microcapsules

Andrea Filler

Santa Clara University, afiller@scu.edu

Jordan Levine

Santa Clara University, jlevine@scu.edu

Jerard Roniel Madamba

Santa Clara University, jmadamba@scu.edu

Natalie Ploof

Santa Clara University, nploof@scu.edu

Follow this and additional works at: https://scholarcommons.scu.edu/bioe_senior



Part of the [Biomedical Engineering and Bioengineering Commons](#)

Recommended Citation

Filler, Andrea; Levine, Jordan; Madamba, Jerard Roniel; and Ploof, Natalie, "Modifying the size of nanopores of alginate microcapsules" (2018). *Bioengineering Senior Theses*. 79.

https://scholarcommons.scu.edu/bioe_senior/79

This Thesis is brought to you for free and open access by the Engineering Senior Theses at Scholar Commons. It has been accepted for inclusion in Bioengineering Senior Theses by an authorized administrator of Scholar Commons. For more information, please contact rsccroggin@scu.edu.

SANTA CLARA UNIVERSITY

Department of Bioengineering

I HEREBY RECOMMEND THAT THE THESIS PREPARED
UNDER MY SUPERVISION BY

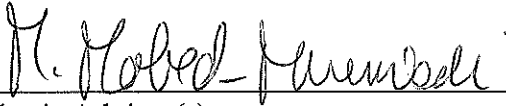
Andrea Filler, Jordan Levine, Jerard Roniel Madamba, Natalie Ploof

ENTITLED

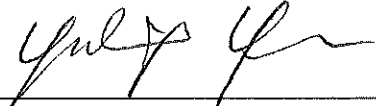
Modifying the size of nanopores of alginate microcapsules

BE ACCEPTED IN PARTIAL FULFILLMENT OF THE REQUIREMENTS
FOR THE DEGREE OF

BACHELOR OF SCIENCE
IN
BIONGINEERING



Thesis Advisor(s) 6/14/18
date



Department Chair(s) (use separate line for each chair) 6/15/18
date

Modifying the size of nanopores of alginate microcapsules

By

Andrea Filler, Jordan Levine, Jerard Roniel Madamba, Natalie Ploof

Senior Design Project Report

Submitted to
the Department of Bioengineering

of

SANTA CLARA UNIVERSITY

in Partial Fulfillment of the Requirements for the degree of
Bachelor of Science in Bioengineering

Santa Clara, California

2017-2018

Abstract

Alginate hydrogels provide desirable biocompatibility and material properties for various biomedical applications, but are limited by the polymer's natural pore size. With the rise of nanotechnology, the desired crosslinked pore size range of 30 nm to 100 nm has not yet been achieved. This project aimed to develop a method to increase the pore size of alginate-based hydrogels in a reproducible manner without compromising their structural integrity. Experimental methods included altering alginate composition using carboxymethyl cellulose or gelatin and inducing conformational changes via Mach-1™ mechanical compression. Fluorescence microscopy was used to visualize the diffusion of FITC-dextran weight markers and fluorescent polystyrene nanoparticles into the microcapsules ($d = 300 \mu\text{m}$) and macrocapsules ($d = 3 \text{ mm}$) for all experimental conditions. Based on pilot experiments, altered alginate composition did not significantly increase the pore size of alginate capsules for the modeled diffusivity range $D = 1 \times 10^{-14} \text{ m}^2/\text{s}$ to $D = 1 \times 10^{-15} \text{ m}^2/\text{s}$. Mechanical compressions did not significantly affect the porosity or diffusivity of alginate macrocapsules ($p > 0.05$) under all conditions for Young's moduli ranging from $E = 76 \text{ kPa}$ to $E = 200 \text{ kPa}$. Based on image analysis results, it could be hypothesized that molecular weight cutoff cutoff may be increased to 500 kDa following 10 successive compressions. Additional work to optimize fluorescent microscopy methods and pore size manipulation methods is required for expanded use of alginate capsules with emerging nanotechnologies.

Acknowledgements

The team would like to thank the following for their support and assistance as we worked on this research project.

We would like to thank SCU School of Engineering for providing the funding and facilities necessary for our project's success.

We would like to thank Adrian Valones, the BIOE Lab manager for 2017-2018, for his generosity in providing lab space and the necessary training for the lab equipment we used over the course of our research.

In a special way, we would like to thank our project advisor, Dr. Maryam Mobed-Miremadi, for her guidance and support over the course of the year. We are grateful for her time and dedication in helping us work towards our research goals.

Table of Contents

Abstract	1
Acknowledgements	2
List of Figures	5
List of Tables	5
List of Abbreviations	5
Introduction	6-11
Background.....	6
Review of Literature.....	7-8
Critics of Current Literature.....	9-11
Statement of Project Goals, Objectives, Expected Results	12-14
Backup Plan.....	13-14
Significance of Project	15-17
Team and Project Management	18-20
Project Budget.....	18
Project	
Timeline.....	19-20
Details of Key Constraints	20
Novel Approaches to Problem	21-24
Supporting Analysis.....	22-23
Expected Results.....	23-24
Materials and Methods	25-34
Materials.....	2
5	
Methods.....	25-34
Results	35-45
Discussion	45-47

Future Directions	48
Summary and Conclusion	49
Engineering Standards and Realistic Constraints	50-51
Bibliography	52-55
Appendices	56-58

List of Figures

- Figure 1. Molecular Structure of Alginate
Figure 2. SEM imaging of TMTD-alginate surface
Figure 3. Molecular structure of crosslinked alginate using divalent calcium ions
Figure 4. Experimental Flowchart for Alginate Pore Size Modification
Figure 5. Mean gray value analysis of diffusion of 70 kDa weight markers into 2% alginate microbeads
Figure 6. Diagram of Measurements for Calculations
Figure 7. Illustration of Mach-1™ set-up
Figure 8. Sample Stress-Relaxation Plots of Crosslinked Alginate using Mach-1™ (from BIOE 140L Winter 2016)
Figure 9. Morphology of Atomized Crosslinked Alginate Microbeads
Figure 10. Gray value plots across alginate microbead diameter
Figure 11. Change in mean gray value of cross-sectional area of alginate microbeads incubated in various fluorescent weight markers
Figure 12. COMSOL modeling of microbead diffusivities
Figure 13. 1D Concentration Profile Plots for 70 kDa and 500 kDa Microbead models
Figure 14. Recovery Time Graphs and Viscoelastic Profiles of Compressed Alginate Macrobeads

List of Tables

- Table 1. Diameters of Hydrogel-deliverable Payloads
Table 2. Pore Sizes of Hydrogels
Table 3. Team Project Management
Table 4. Alginate and CaCl₂ variations
Table 5. Alginate-Gelatin Compositions [1.5% CaCl₂]
Table 6. Confirmed Diffusion of Fluorescent Dyes in Macrobeads and Microbeads, uncompressed and compressed
Table 7. Estimated Microbead Diffusivities based on COMSOL modeling
Table 8. Material Properties of Compressed Alginate Microbeads

List of Abbreviations

AA: Alginate	PA: Polyacrylamide
AFM: Atomic force microscopy	PS: Polystyrene
C: Compression	PLA: Polylactic acid
CL: Crosslinker	RFU: Relative Fluorescence Units
FITC: Fluorescein isothiocyanate	SEM: Scanning electron microscopy
HA: Hyaluronic Acid	TMTD: triazole-thiomorpholine dioxide

Introduction

Background

With the rise of modern medicine and an emphasis on prevention and treatment of various diseases, hydrogels and nanotechnology have risen to the forefront of biomedical research. Hydrogels, biomaterials with characteristics that closely mimic *in vivo* conditions, are a promising technology that have applications in drug delivery, therapeutics, diagnostics, and cell repair [1]. With a wide range of characteristics and both natural and synthetic origins, hydrogels can be manipulated to meet a number of biomedical needs [2]. Additionally, the advent of nanotechnology has greatly expanded the biomedical field, enabling focus on a smaller scale [3]. With a growing concentration on repairing, replacing, and regenerating the human body, there is now a demand for a biocompatible material that can safely, efficiently, and sustainably encapsulate and deliver a variety of biological and chemical payloads, including nanoparticles [4].

Alginate has been a particularly promising option because it is naturally biocompatible, bioinert, low-cost, and has a structural composition that closely resembles *in vivo* environments [5]. As a result, alginate is a strong candidate for applications ranging from drug delivery and therapeutics to diagnostics and cell repair [1][5]. Alginate can safely interact with a number of payloads including cells, chemical drugs, biological molecules, and synthetic technology, while preserving the structural integrity and functionality of these payloads to increase their therapeutic efficacy [4].

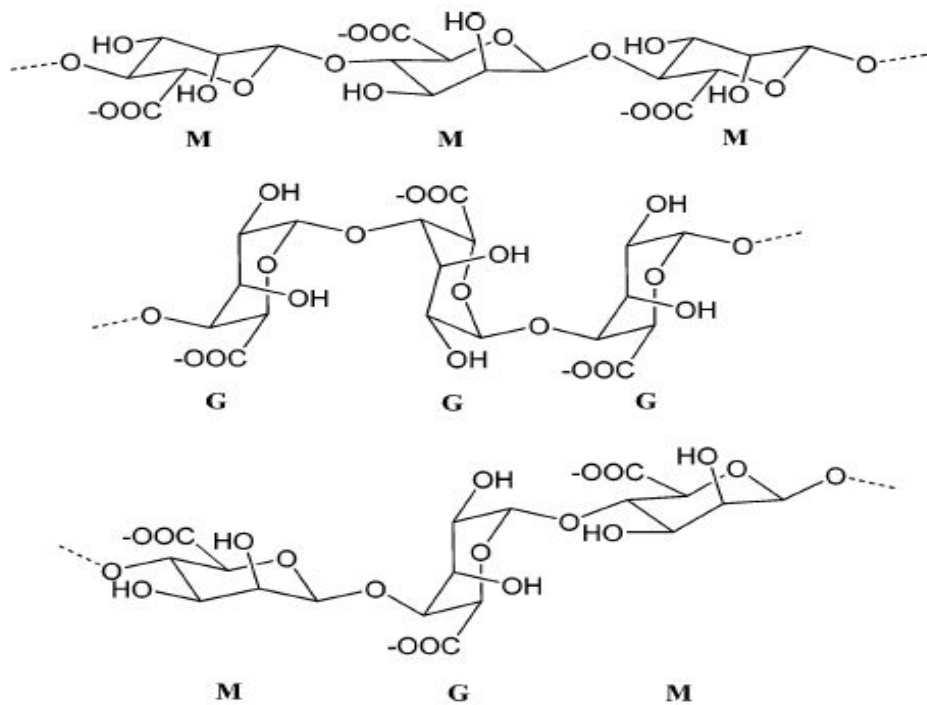


Figure 1. Molecular Structure of Alginate. Mannuronic acid (M) and guluronic acid (G) residues are labeled [1]

Review of Literature

Biomaterials have long been used to replace tissue lost to disease or trauma, and are designed to be bioinert [5]. Hydrogels, a class of biomaterials, have emerged as promising candidates for biomedical applications, including tissue engineering, and drug delivery [2][5]. Hydrogels consist of crosslinked macromolecular networks, and have varying properties depending on their intramolecular interactions and compositions, altering their physical and chemical properties [5]. Tunable characteristics and the ability to simulate *in vivo* conditions make hydrogels a desirable biomaterial, as most hydrogels have impressive water retention capabilities, biocompatibility, porosity, and comparable stiffnesses to that of soft tissue [2][5][6][7]. The porosity of these hydrogels can determine their applications and efficacy in drug delivery or tissue engineering. [2][7]. Applications in tissue engineering require hydrogels with pore sizes in the order of microns. The techniques for pore manipulation on the micron-scale have been

established by previous research, and are less concerned with pore-size exclusion [2]. However, pores of several microns are too permeable for applications that require controlled diffusion rates or pore-size exclusion.

Table 1. Diameters of Hydrogel-deliverable Payloads [8]

Payload	Diameter
Proteins	1-5 nm
Small Chemical Drugs	< 1 nm

Liposomes	20-50 nm
Exosomes	30-100 nm
Nanoparticles	<100 nm

Condensed Plasmid DNA	100 nm
Cells	>50 μ m

Drug delivery systems that utilize hydrogel encapsulation allow for the delivery of the therapeutic payload while protecting it from external conditions [7]. Payloads can consist of proteins, which are most commonly around 1-5 nm in diameter, and nanoparticles, defined to be particles <100 nm in diameter [8]. Diffusion of these payloads out of the hydrogel can be modulated by hydrogel composition and the method of manufacturing.

Critics of Current Literature

Hydrogels of interest for this study are hyaluronic acid, collagen, polyacrylamide, and alginate, as all have been established as suitable for biomedical applications. Among these hydrogels, alginate is arguably the best candidate for molecule payloads of 100 nm and smaller.

Hyaluronic acid (HA) is a proteoglycan that is one of the primary components of the extracellular matrix and is desired for its resilience and hydrodynamic properties. The porosity of HA is on the micron scale, giving it an advantage as a candidate for biomaterial scaffolding in tissue engineering applications but disadvantaging it in the realm of drug delivery and pore-size exclusion applications [6]. Collagen, a structural protein of the ECM and another widely used polymer, also features porosity on the micron scale and is likewise more suited for tissue engineering applications [9].

Polyacrylamide (PA) is a synthetic polymer that is biocompatible, inert, and features a crosslinked nanopore size approximately 10 nm in diameter [10]. The manufacturing of PA microcapsules is also well documented [10][11]. As a result, PA hydrogels seem to be another suitable candidate. While the porosity of PA can accommodate most other nanoparticle payloads, the methods to produce PA hydrogels and microcapsules yield results with high variabilities of success. PA hydrogel and microcapsule production requires a number of reagents, some of which are cytotoxic, and specific conditions to ensure the quality of the capsules [10][11].

Alginate, a natural polymer, has a crosslinked pore range of 3-10 nm and can already accommodate the diffusion of lower MW proteins (less than 70 kDa) and other small molecules [5]. Established biofabrication methods include polyelectrolyte complexation using atomization, inkjet bioprinting, electrostatic spraying, on-chip synthesis [12] and

more recently nanoimprinting [13]. Alginate is also noncytotoxic [5], enabling its expanded use in *in vivo* applications. Recent research on alginate hydrogels has also shown that it can be treated with triazole-thiomorpholine dioxide (TMTD) to produce a hydrogel that is completely nonimmunogenic [14]. Other hydrogels, such as HA and PA, suffer from immunogenicity *in vivo*, which causes albumin to adhere to the surfaces of these hydrogels [5] [14]. Albumin interactions with hydrogel microcapsule surfaces could interfere with the effective porosity of the microcapsule by clogging the pores and restricting diffusion into and out of the microcapsule. Using TMTD-alginate could allow for an expanded role of *in vivo* alginate hydrogels to deliver larger payloads in consistent ways. However, because the natural pore size of alginate is approximately 5 nm, it cannot currently deliver therapeutic payloads reliably or allow the inward diffusion of molecules other than proteins.

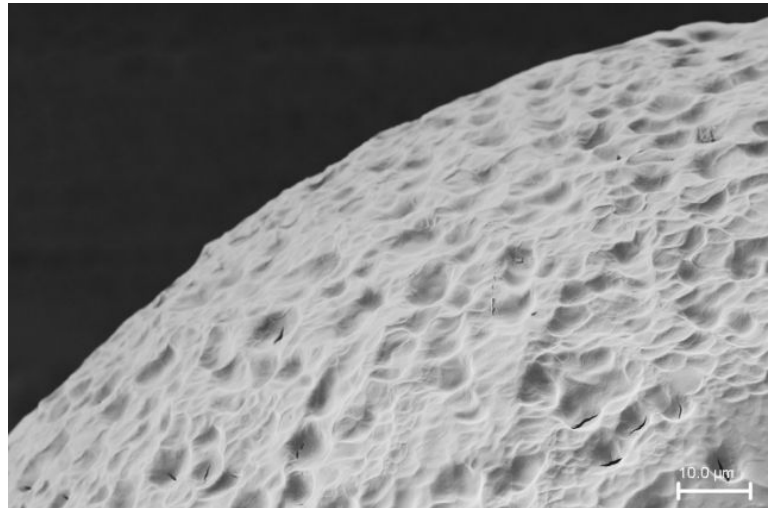


Figure 2. SEM imaging of TMTD-alginate surface [14]

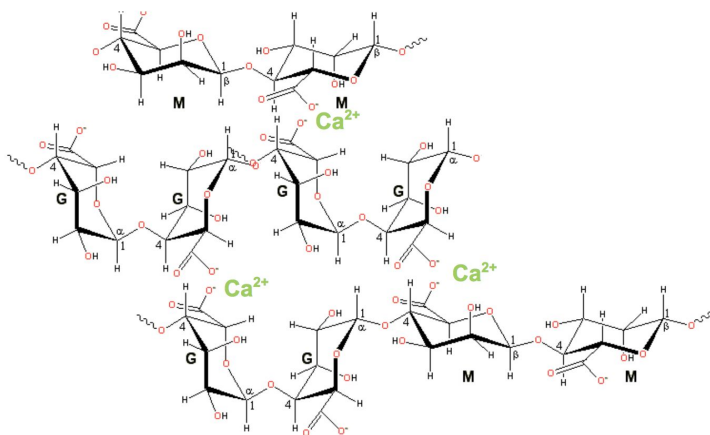


Figure 3. Molecular structure of crosslinked alginate using divalent calcium ions. [1]

Previous approaches have been pursued to tailor the pore sizes of hydrogels, such as modifying polymer molecular weight, co-polymerization of two or more polymers, and lyophilization [2][7]. For alginate, research has been conducted on modifying its pore size within the micron scale for applications in tissue engineering, but little to no research has been conducted in regard to the nanopore scale or on methods for reliable and predictable nanopore size manipulation. Alginate pore size could be modulated by using alginates of different molecular weights, adjusting the ratio of mannuronic (M) and guluronic (G) acid residues and changing crosslinker concentration as well as crosslinking time [1]. However, these processes have not yet been standardized to yield predictable pore sizes. In addition, previous student research conducted at Santa Clara University has also shown that mechanical compression is an effective method for increasing nanopore size. [15][16] This conclusion still needs to be validated and quantified in order to achieve predictable results moving forward and eventual standardization [15][16].

Table 2. Pore Sizes of Hydrogels

Alginate	Collagen	Hyaluronic Acid	Polyacrylamide
5 nm [5]	>1 μm [6]	>1 μm [9]	10 nm [10]

Statement of Project Goals, Objectives, Expected Results

Alginate is a viable candidate for fulfilling the market need, but its crosslinked pore size is too small for most applications. Additionally, there is currently no standard method for uniformly manipulating pore size in alginate hydrogels. Therefore, our research has two main objectives:

1) Increase molecular weight-cut off of alginate-based hydrogels without causing damage to the structural integrity of the crosslinked structures

Our primary means of expanding the pore size to a range of 10 to 30 nm will be via compression and relaxation cycles using the Mach-1™ mechanical testing device, which have been shown to modify pore sizes [17]. For our purposes, damage to the structural integrity of the microcapsules will be observations of microcrack formation on their surface. Atomic force microscopy (AFM) and scanning electron microscopy (SEM) will be used to verify that our microcapsule manipulations are not inducing such degradation. If AFM and/or SEM images present any indication that our methods are degrading the microcapsules, then new methods will be explored. If we find that mechanical compression has severely compromised the structural integrity of the microcapsules, we will explore two additional methods: lyophilization and the manipulation of the ratio of residues constituting alginate. The former has been shown to increase pore sizes. However, research has been limited to pore sizes in the micron scale [2]. For the latter method, pore sizes can be expanded, but currently they cannot be made uniform according to the desired pore size [1].

2) Devise a tool kit to test the incremental increase of pore size using standardized nanoparticles

Fluorescent nanoparticles of varying sizes will be used to confirm modified pore sizes and establish subsequent diffusion rates both into and out of alginate microcapsules.

Such a kit would utilize pore size exclusion properties to indicate the uniformity in pore size expansion as well. Achieving pore sizes in our desired range would optimally situate such alginate microcapsules for the delivery of nanoparticles, small molecules, and therapeutic payloads. Additionally, by standardizing a process of incremental pore size expansion and subsequent diffusion rates, therapeutics in the form of polymers, combined with inorganic materials, polymeric materials, and carbon based nanomaterial [17] could be delivered *in vivo* in a time-delayed manner.

Backup Plans

3D Printing

If insurmountable difficulty arises using the physical and chemical modifiers to increase pore size, we will turn to a 3D-printed solution. 3D-printed grids would act as artificial pores, as they would be coated with a thin layer of minimally crosslinked alginate. Cells, as well as nanoparticles or other small molecules, could easily be encapsulated inside the gridded chamber for diagnostic applications or drug delivery purposes.

The material used to print the grids would be polylactic acid (PLA). PLA is a biodegradable thermoplastic made from natural resources. It has a relatively low melting temperature compared to other plastic filaments which allows it to be printed onto a non-heated platform fairly easily [18]. Additionally, because of this low melting temperature, PLA is less susceptible to sudden temperature shifts and subsequently less prone to cracking or warping than other commonly used filaments [18]. A number of studies have already used PLA in conjunction with alginate, predominantly for tissue engineering solutions, indicating that the thermoplastic is a viable biocompatible option [19]. The plastic grids would be printed using the Ultimaker 3D printer in the Santa Clara University Maker Lab. This machine has a resolution of 20 microns, which is 1000x larger than the nanometer range we are trying to achieve [20]. To produce artificial pores in the 10-30 nanometer range, we would stack multiple PLA grids on top of each

other to reduce the grid size until the desired pore size was reached. Adhesion between layers of PLA is well-established in literature and easily accomplished [18]. Final pore size could be verified via microscopic imaging. While this method would not modify the pore size of the crosslinked alginate itself, it could be used to explore applications that require nanoscale pores.

Lyophilization

Our second backup plan will be lyophilization, or freeze-drying. Lyophilized alginate-based hydrogels have been used in tissue engineering applications, and their lyophilization methods established [2]. Currently, collagen-chitosan hydrogels have been shown to be biocompatible *in vivo* after lyophilization [2]. Porosity has also been shown to have been manipulated by different lyophilization profiles, but most manipulations have been performed for alginate scaffolds intended for tissue culturing applications. As such, all pore size manipulations have occurred at the micron range [2][7]. Lyophilization may yield appropriate nanopore manipulations in smaller scale alginate constructs, e.g. macrobeads and microbeads. Our alginate-based constructs will be placed inside a lyophilizer, and rapidly cooled in order to bring its water content from the liquid phase to the solid phase. Next, the pressure within the lyophilizer will be decreased to dehydrate the hydrogel via sublimation, with the intention of increasing the pore size [2]. The mechanical properties and the rate of degradation of the final lyophilized product are most affected by the initial chemical composition and molecular weight of the macrobeads.

Significance of Project

Diagnostics

Encapsulation of cells in alginate membranes has a variety of *in vivo* and *in vitro* diagnostic applications. Because alginate is a naturally-derived biocompatible material, it does not elicit any immune response from its host. For this reason, various cell types encapsulated in alginate microcapsules could be implanted into a host without fear of degradation or antibody recognition [21]. This would allow for analysis of *in vivo* functioning of various modified cell systems. Alginate encapsulation also has promising *in vitro* applications for drug and other diagnostic testing. Due the matrices that exist in the calcium crosslinked form of the material, encapsulated cells are able to engage in extracellular interactions reminiscent of those that occur *in vivo* [22]. Biomembrane encapsulation also increases the longevity of cell viability by facilitating nutrient diffusion in and waste removal out of the capsule [22]. Alginate-encapsulated cells could be exposed to a solution containing a particular drug; the rate of diffusion of the drug, and consequently the effective concentration “seen” by the cell, could be manipulated based on the pore size of the alginate. This would be valuable in determining the time-dependent toxicity of a particular drug.

Drug Delivery

Drug delivery is arguably one of the most prevalent applications for alginate microcapsules. With a growing pharmaceutical industry, there is a significant market for safe, efficient, and cost-effective delivery methods. Nanoparticle-hydrogel hybrid systems integrate two systems, nanoparticle therapies and hydrogel formulations to address various biological and medical challenges [4]. Precise control over drug quantity and release rate is advantageous over conventional drug release because of enhanced bioavailability and minimized side effects [17]. There has been growing interest in designing advanced hydrogels with tunable properties, especially porosity, to optimally release nanoparticles for therapeutic benefit [17]. Because the average natural

pore size of alginate (5 nm) is too small for most nanoparticles to diffuse through, nanoparticle delivery methods involving alginate hydrogels rely on tuning degradation, swelling, or dissolution to control drug release [17][23]. Being able to increase the pore size of alginate in a predictable manner could introduce additional ways to modulate diffusion rates out of nanoparticle-alginate systems. Combined with the relative ease of manufacturing alginate microcapsules and the physical and chemical characteristics of alginate, more efficient drug delivery systems can be developed to address more biological and medical issues [17].

Wound Healing

Hydrogel pads are a novel form of wound dressing that come into direct contact with a wound to promote healing. Hydrogels generally serve the dual purpose of maintaining moisture in the wound area for faster wound repair, and absorbing wound exudate [24]. They also serve the purpose of releasing biomolecules, such as antibiotics to promote wound repair [25]. Alginate hydrogels have been used for wound healing due to their biocompatibility, and their absence of cytotoxicity. Applications using hydrogels containing alginate alone, however, are restricted to wound repair that does not require a long period of time, as they are degraded by absorbing alkaline media, such as wound exudate [26]. Altering the porosity of alginate by coating the hydrogel with chitosan can control the steady release of these biomolecules to counter the degradation caused by absorbing wound exudate [27].

Bioenergy

Alginate has been applied in the bioenergy sector as a component for the production of biodiesel. Biodiesel is an environmentally-friendly form of energy that has grown in popularity [28]. One method of producing this renewable source of fuel is lipase catalyzed transesterification, but some of the drawbacks of this method of biodiesel production are the lack of stability of lipase during processing and the difficulty in recycling lipase from the reaction mixture [28]. As a result, alginate has been used to

physically entrap lipase to improve its stability [28]. Other biofuel production methods using biomolecule entrapment involve alginate co-immobilization with other polymers, adjusting the entrapment parameters necessary for efficient biofuel cell design [29]. Changing the porosity of alginate by mechanical means in a predictable way would greatly improve manufacturing efficiency and simplicity by reducing the number of reagents needed to produce the entrapping membrane and simplifying production procedures. In addition, new applications involving larger entrapped biomolecules could be developed to improve the efficiency of biofuel cells.

Desalination

Desalination processes produce drinkable water by removing salts from seawater, saline groundwater, and wastewater at the cost of significant energy consumption [30]. Contributing to the energy costs of desalination is membrane fouling due to the buildup of microbes, dissolved solutes and suspended solids [30]. Studying this phenomenon to make desalination more energy-efficient is hampered by insufficient models of membrane fouling [30]. Alginate is used as a model material to study membrane fouling, but the variance in pore size measurements produces errors in biofouling models as a result of estimations that vary by measurement technique [30]. Predictably producing pore size would allow for more accurate determination of membrane parameters, like water and salt fluxes across the membrane, in order to establish better membrane fouling models [30]. Working towards these better models could allow for more efficient desalination methods that may benefit those in water-scarce locations [30].

Team and Project Management

Due to the limited research on porosity manipulation in alginate, the scope of the project is relatively broad. As a result, team management and organization are imperative. We have identified four project components (professional communication, literature search, lab experimentation, and written communication) that have been further broken into individual roles. A summary of team management and roles can be seen below:

Table 3. Team Project Management

Project Component	Role	Responsible Team Member
Professional Communication	Primary Contact	Jerard Madamba
Literature Search	Biofabrication	All Team
	Mechanical Manipulation	All Team
	Methacrylation	Natalie Ploof
	Gelatin	Andrea Filler
	Lyophilization	Jerard Madamba
	UV	Jordan Levine
Lab Experimentation	All Techniques	All Team
Written Communication	Figures	Jerard Madamba
	Citations	Natalie Ploof
	Formatting	Jordan Levine
	Submissions	Andrea Filler

Project Budget

The estimated budget for this project and amount provided by SCU's School of Engineering Undergraduate Programs Senior Design Grants is \$1,930.30 (Appendix

1.1). The cost of our primary reagent, alginate, along with the materials to modify its structure, are relatively inexpensive. A single experimental batch will only require 3 mL of alginate to produce approximately 300,000 beads, resulting in a cost of about 2.5 cents per batch. The most costly reagents are the fluorescent size markers and nanoparticles that will be used to test the size and uniformity of the pores following modification, constituting just under 30% of the total budget. The components used to manufacture the alginate microcapsule consistently, the flowmeter and needles, will comprise about 50% of the overall budget, but will be crucial for producing accurate, replicable results. Much of the high-cost equipment associated with mechanical modification, crosslinking alternatives, and imaging are already present in the Bioengineering laboratories and were not included in the project's budget considerations.

Project Timeline

This project will be completed over the course of 30 weeks. The first five weeks will be devoted primarily to a review of relevant literature. From this literary research, unfulfilled needs in the current field will be identified, as well as preliminary protocols for achieving pore modification. A list of reagents and equipments will be assembled and ordered by the end of Fall Quarter (week 10). Lab safety training and familiarization with basic lab protocols will be completed by all team members during Fall Quarter as well.

Experimentation in lab will commence at the end of Fall Quarter with the majority of lab work taking place during Winter. Any residual experimentation after week 20 will be completed in the first few weeks of Spring Quarter. Data analysis will begin around the third week of Winter Quarter and persist for a couple of weeks after the conclusion of experimentation (week 24). As results from initial experimentation and method optimizations are interpreted, development of standardized protocols will begin (approximately week 17). These standardized protocol will be reviewed and tested during the first two weeks of Spring Quarter. The final report summarizing research

findings and including standardized protocols will be written primarily during Spring Quarter and completed by week 28.

Details of Key Constraints

Our first design-related constraint concerns the structural integrity of the microcapsules produced. To produce microcapsules that are uniformly spherical, both the concentration of the alginate solution and the concentration of the crosslinking solution must be high enough to maintain their structural integrity. As an example, concentrations as low as 0.5% for sodium alginate solution and 0.5% for crosslinker may not create hydrogel samples with adequate mechanical properties. If alginate concentration and/or crosslinker concentration is too low, the resultant hydrogel may not be manipulatable or may prematurely deform due to its fragile constitution. Therefore, any attempts to reduce pore size by reducing the composition of alginate or its crosslinker are limited by the minimum concentration of each reagent required for the microcapsule to maintain its physical form.

Our second constraint concerns the accuracy of our measured pore sizes. Pore sizes of the microcapsules will be estimated by the diameter of the molecular weight markers that successfully diffuse through them. Experimental procedures for this project shall involve FITC-dextran weight markers of varying molecular weights or nanoparticles sized 26 nm and 47 nm, respectively. One limitation of this project is that pore sizes besides those matched by these weight markers need to be extrapolated using mathematical models. Therefore, we will not be able to accurately measure any pore sizes between these two diameters. Rather, pore sizes of each hydrogel condition will be estimated using mathematical extrapolation assuming steady state diffusion.

Novel Approaches to the Problem

Our approach to increase the pore size of alginate involves the manipulation of alginate hydrogel composition as well as post-production modifications. Review of current literature on alginate hydrogels reveals that pore size characteristics for different alginate hydrogel formulations are inconsistent throughout the field. Therefore, most experimentation performed as part of this project is focused on characterizing the porosity of different alginate-based hydrogel formulations and the effects of mechanical manipulations on the pore sizes of these hydrogels. Experimentation shall proceed as outlined in Figure 4.

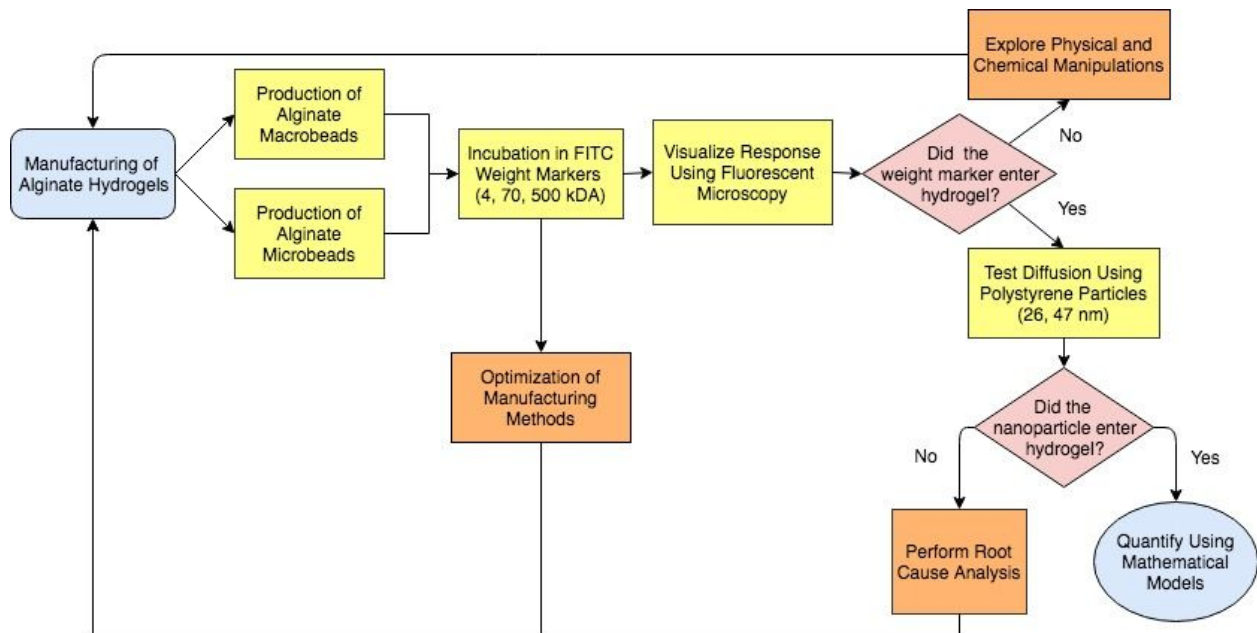


Figure 4. Experimental Flowchart for Alginate Pore Size Modification

Experimentation shall begin with pilot experiments to determine the diffusion behavior of FITC fluorescent markers across a hydrogel/saline interface. Hydrogels prepared for this pilot experiment shall vary by alginate and crosslinker concentrations, and production shall begin with the formation of macrobeads and slabs, followed by microbeads for more comprehensive analysis. Based on qualitative analysis of

fluorescent microscopy, iterations of hydrogel composition and manufacturing methods will be explored and the resultant findings characterized.

For the pilot experiment, qualitative evaluation of diffusion performance shall focus on fluorescence microscopy to visualize the behavior of 70 kDa and 500 kDa weight markers, which correspond to pore sizes of 5-6 nm and 10-11 nm, respectively [17]. Emphasis on these weight markers indicates successful pore size modification from the baseline condition (3.0% w/v alginate crosslinked in 1.5% w/v CaCl₂). Conditions in which the weight markers successfully enter the hydrogel shall be prioritized for iteration, as this would indicate achievement of target pore size. If all conditions in the pilot experiment fail to allow the diffusion of the weight markers, or if the results of this pilot experiment are ambiguous as to whether or not the weight markers successfully diffuse, then alternative methods for hydrogel production will be explored, including, but not limited to, hydrogel formulation, crosslinking time, crosslinking methods (e.g. methacrylation, photocrosslinking), and post-crosslinking modification (e.g. mechanical compression).

Experimentation past the pilot study shall then proceed using alginate microbeads produced using atomization. Microbeads created for these experiments will be approximately 300 µm in diameter and produced in large batch sizes, aiding in the validation of uniformity among samples.

Supporting Analysis

Modification of alginate microbead pore size will be characterized using analysis of fluorescent microscopy. Images of diffusion behavior taken at multiple timepoints will be analyzed using appropriate software to quantify relative fluorescence units (RFU) throughout a region encompassing an alginate/buffer interface. RFU values shall then be incorporated into mathematical modeling to characterize the rate of diffusivity and

pore sizes of the alginate hydrogel. In addition, SEM shall enable qualitative visualization of the surface topography of the hydrogels to validate the structural integrity of the alginate construct.

Expected Results

Success in reaching the aforementioned goal of increasing the pore size of alginate hydrogels shall be validated using the following methods. First, visual verification by fluorescence microscopy shall be used as a preliminary screen to determine successful pore size manipulation. Based on the objectives previously outlined, success at this stage will be defined as the entry or escape of 500 kDa FITC weight markers and 26 nm polystyrene nanoparticles into or out of the alginate hydrogel. Second, SEM imaging must demonstrate no indications of damage (i.e. microcracks) to the hydrogel, affirming that all diffusive behavior is caused by intact micropores only. Third, analysis of fluorescent microscopy images will be used to quantify diffusion at the hydrogel/buffer interface using Fick's First and Second Laws of Diffusion, assuming steady state diffusion. Fick's First Law (Equation 1) in 1D and Cartesian coordinates states:

$$J(x) = -D \left(\frac{\partial c(x)}{\partial x} \right) \quad (1)$$

where $J(x)$ is the flux at the hydrogel/buffer interface, D is the diffusion coefficient, and $\frac{\partial c(x)}{\partial x}$ is the concentration gradient. Fick's Second Law (Equation 2) states:

$$\frac{\partial c(x,t)}{\partial t} = -D \left(\frac{\partial^2 c(x,t)}{\partial x^2} \right) \quad (2)$$

where $\frac{\partial c(x,t)}{\partial t}$ is the rate of concentration change over a given distance and time, D is the diffusion coefficient, and $\frac{\partial^2 c(x,t)}{\partial x^2}$ is the curvature of the concentration gradient.

Fick's Second Law can also be written in spherical coordinates (Equation 3) in order to account for spatial scale assuming that diffusion in the angular dimensions is constant:

$$\frac{\partial C_m}{\partial t} = \frac{1}{r} \frac{\partial}{\partial r} \left(D_e r \frac{\partial C_m}{\partial r} \right) \quad (3)$$

Where $\frac{\partial C_m}{\partial t}$ is the rate of concentration change over a given distance and time, r is the given distance over which diffusion occurs, D_e is the effective diffusivity of the solute, and $\frac{\partial C_m}{\partial r}$ is the concentration change over the given distance. As r increases, the rate of concentration change decreases, indicating that diffusion is more rapid over shorter distances. Therefore, the diffusion of fluorescent dyes into microbeads will be more easily visualized than diffusion of fluorescent dyes into macrobeads. Concentration gradients will be determined using image analysis of fluorescent microscopy in ImageJ. Calculated diffusion constants will be compared with existing literature documenting associated diffusion constants for different micropore sizes. Based on this mathematical modeling method, alginate hydrogel pore size will be empirically extrapolated.

Materials and Methods

Materials

Medium viscosity sodium-alginate, (listed as “alginic acid sodium salt from brown algae,” A2033), anhydrous sodium chloride (793566), anhydrous calcium chloride (C1016), 4 kDa FITC-dextran (FD40S), 70 kDa FITC-dextran (FD70S), and 500 kDa FITC-dextran (FD500S) markers were purchased from Sigma Aldrich. 26 nm and 47 nm polystyrene fluorescent beads were purchased from Thermo Fisher. Additionally, a flowmeter was purchased from Omega (FL-9301). Finally a custom concentric atomizer needle (inner gauge: 24G; outer gauge: 16G) was purchased from ramé-hart Instrument Co. Additional materials including a Mach-1™ device from Biomomentum, Olympus CKX53 fluorescent microscope, and syringe pump were already present in the SCU Bioengineering laboratories.

Methods

Macrobead Formation [31]

Medium viscosity sodium alginate was dissolved in 0.9% NaCl solution and allowed to spin for 24 hours. 2 mL of the alginate solution was then drawn up into a 10 mL disposable syringe and a 22 G blunt needle was attached to the end of the syringe. The alginate solution was then manually ejected from the syringe into a 60 mm petri dish filled to half of its volume with CaCl₂. Macrobeads were then allowed to crosslink for 30 minutes. Following a 30 minute crosslinking session, beads were rinsed with 12 mL of 0.9% NaCl three times. During each rinse, the NaCl solution was added to the 60mm petri dish and was drained. Following the third wash, 12 mL of 0.9% NaCl was added to the dish to prevent the beads from drying out.

Macrobeads were later fabricated using a syringe pump in order to improve uniformity and replicability. Medium viscosity sodium-alginate was dissolved in 0.9% NaCl and

allowed to spin for 24 hours. 2 mL of the alginate solution was then drawn up into a 10 mL disposable syringe and a blunt 22 G needle was attached to the end of the syringe. The alginate solution was then ejected into a CaCl_2 bath in a 60 mm petri dish from a height of 7 cm at a constant rate of 1.0 mL/min. Beads were left to crosslink for 30 minutes. Following crosslinking, beads were rinsed three times in 12 mL allotments of 0.9% NaCl. After the third rinse, the beads were submerged in 12 mL of 0.9% NaCl to prevent drying.

Atomization of Microbeads [1]

Following pilot experimentation, methodology switched to formation of microbeads to improve bead uniformity, replicability, and biological relevance. These beads have diameter around 300 microns. For microbead formation, sodium-alginate was dissolved in 0.9% NaCl and allowed to spin for 24 hours. 1 mL of the alginate solution was pulled up into a 3 mL lock-syringe and the syringe was then fitted with a custom atomizer needle assembly with a concentric 24 G needle surrounded by a 16 G needle. The assembly was then loaded into a syringe pump and the sodium-alginate mixture was passed through the needle into a CaCl_2 crosslinker bath from a height of 3 cm. The air (F_A) and liquid (F_L) flow rates were adjusted to 1.5 mL/min and 1.0 mL/min, respectively and beads were crosslinked for 1 hr. The microbeads were then washed three times in excess 0.9% NaCl using a sieve. The beads were then transferred to a 60 mm petri dish and submerged in 12 mL of 0.9% NaCl to prevent drying.

Slab Formation [1]

Medium viscosity sodium-alginate was dissolved in 0.9% NaCl and left to stir for 24 hours. The mixed alginate solution was then pipetted into 12-well plates, filling each well approximately half way. The alginate slabs were allowed to dry to a thin film. Drying time varied by slab diameter and thickness as well as slab composition (i.e. weight percent of alginate). Once drying was complete, the wells were filled with CL. Slabs were allowed to crosslink for 1 hour before being removed and placed into 60 mm petri

dishes for rinsing. Each slab was rinsed three times in 12 mL of 0.9% NaCl each rinse. After the third rinse, the slabs were submerged in 12 mL of 0.9% NaCl to prevent drying.

Fluorescent Imaging

FITC fluorescent weight markers were dissolved in 0.9% NaCl at 1 mg/mL. Polystyrene fluorescent beads were diluted in 0.9% NaCl at a 1:10 dilution to achieve a concentration of 1 mg/mL. All fluorescent dyes were prepared in 5 mL batches. Fluorescent microscopy and image capture were performed using the Olympus CKX53 microscope in conjunction with the Olympus cellSens platform. A blue filter block (excitation 488 nm, emission 509 nm) to visualize fluorescent dyes.

Encapsulation

Fluorescent dyes were incorporated into alginate solutions prior to crosslinking in CaCl_2 . The alginate-dye mixtures were then used to form macrobeads, microbeads, or slabs. Following crosslinking, the alginate constructs were washed three times in 0.9% NaCl. Each wash was transferred to and stored in 15 mL Eppendorf tube wrapped in aluminum foil to prevent photobleaching. For image analysis, the washes were transferred individually to 60 mm petri dishes.

Rapid Diffusion Tests

Alginate constructs were isolated on a microscope slide (slabs and microbeads) or within a well plate (macrobeads). For isolation, sections of slabs were cut into circles approximately 1 cm in diameter and physically secured to the microscope slide using tape. Macrobeads were isolated in a flat-bottom 96-well plate (one bead per well) and excess saline solution was pipetted out. Microbeads were isolated onto a microscope slide by pipetting approximately 20 μL of microbead suspension onto the slide. Microbead morphology prevented complete isolation of the constructs from the saline buffer, so all fluorescent testing on microbeads was performed in saline buffer.

After the alginate constructs were isolated, approximately 10-20 μL of fluorescent dye was added adjacent to the slab, macrobead, or microbead suspension such that an alginate-dye interface could be visualized by microscopy. Images were captured at 60 second intervals over 300 seconds using the cellSens platform, starting upon application of the dye. Images were exported for analysis by ImageJ.

24-hour Incubation

Rapid diffusion methods were repeated as above, but alginate constructs were fully submerged in fluorescent dyes for an additional 24 hours and reimaged to determine long-term diffusion behavior. Images were exported for analysis by ImageJ.

Image Analysis

Qualitative Analysis of Microbead Diffusivity

ImageJ analysis was used to determine the relative fluorescence of the alginate constructs at the beginning and end of the testing period (rapid diffusion or 24-hour incubation). Images were exported into ImageJ and converted into grayscale. Gray value profiles were plotted along a fixed line spanning the alginate-dye interface. Areas of high fluorescence were indicated by higher gray values, while areas of low or no fluorescence were indicated by lower gray values. Profiles for each image captured during each experiment were generated and compiled for qualitative analysis. Diffusion of the tested weight marker/fluorescent bead into the alginate construct was determined based on qualitative comparison of each successive profile. Progressive increases in gray value, relative to background, at the alginate-dye interface and in regions within the construct corresponded with diffusion of the dye into the construct. Unsuccessful diffusion of the dye corresponded with no noticeable increase, relative to background, in gray value at the alginate-dye interface and in regions within the construct. Pore size estimations were made based on the observed diffusive behavior of the weight marker/fluorescent bead.

Quantitative Analysis of Microbead Diffusivity

In addition to the qualitative results supplied by the gray value profiles, a quantitative analysis was applied to microbead fluorescence images. For each compression condition and weight marker, the elliptical tool in ImageJ was used to outline a single representative microbead at t=0 minutes. This selection was copied to the image taken under the same conditions at t=10 minutes (Figure 5). Using an ImageJ analysis function, the mean gray values were calculated over the selected area for both timepoints.

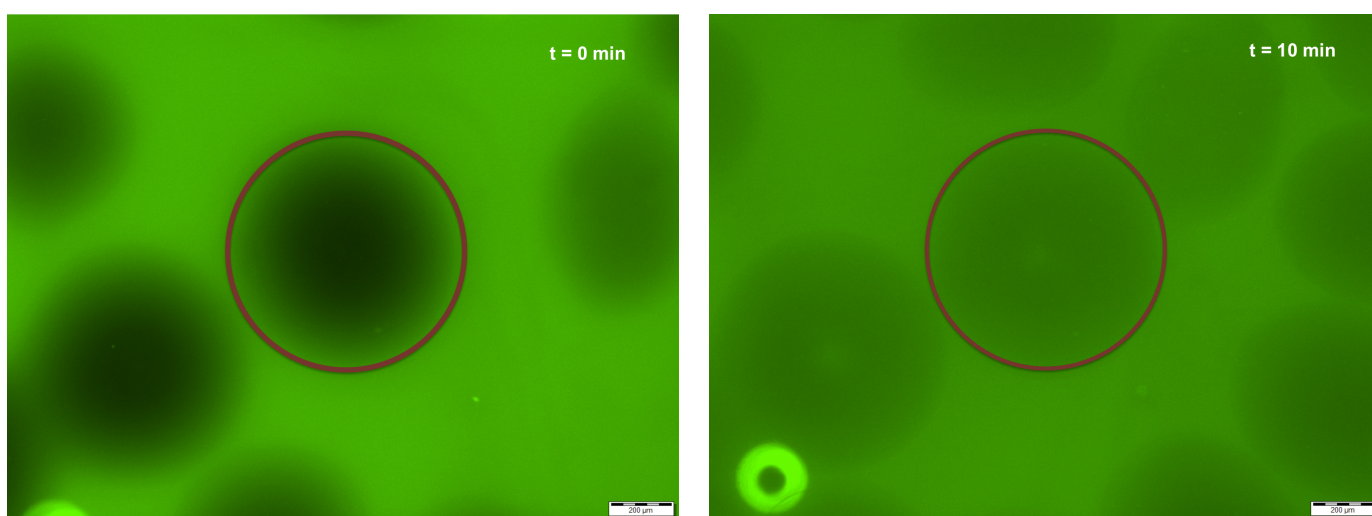


Figure 5. Mean gray value analysis of diffusion of 70 kDa weight markers into 2% alginate microbeads.

Quantitative Analysis of Macrobead Diffusivity

The following measurements were obtained from macrobead diffusion images using the cellSens platform: mean radial diffusion distance and estimated total bead cross-sectional area. From the area, the assumed total bead radius was calculated. The radius of the region where diffusion did not occur was calculated as the total radius minus the radius of diffusion. Ratios of no-diffusion radii to total bead radii were subsequently calculated.

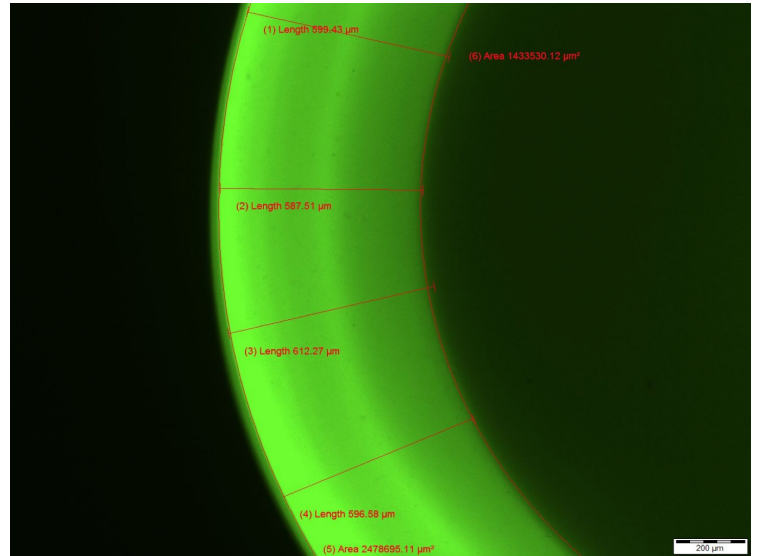
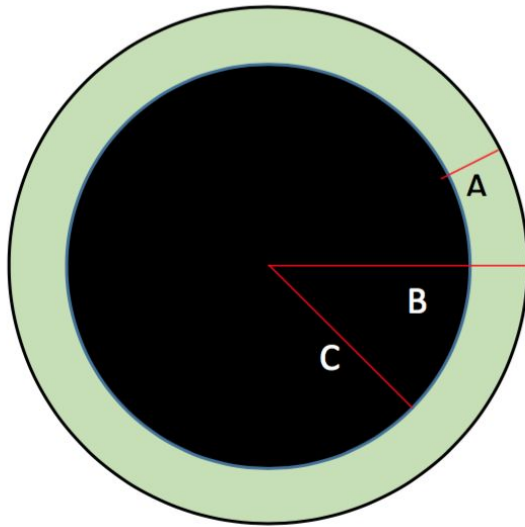


Figure 6. Diagram of Measurements for Calculations. Left: Measurements of radial distance of diffusion (A) were obtained from microscope images. From the total area of the bead, the assumed total radius of the bead was calculated (B). The radius of the region where diffusion did not occur (C) was calculated as the total radius minus the radius of diffusion (B-A). Right: Fluorescent microscopy of macrobead semisphere incubated in FITC-dextran. Measurements were taken using built-in tools in cellSens. Distance A was averaged for each bead using multiple measurements per region.

Statistical Analysis

Microbeads

Mean gray values obtained from replicates of the same compression conditions and weight marker incubations were averaged to obtain a single value. A Student's *t*-test was performed on these averaged values to determine if a significant difference in mean gray value, or fluorescence intensity, existed between $t=0$ and $t=600$ seconds timepoints for a given compression condition. An independent, two-sample *t*-test assuming equal variance was performed:

$$t = \frac{\bar{X}_1 - \bar{X}_2}{s_p \sqrt{\frac{2}{n}}} \quad \text{where} \quad s_p = \sqrt{\frac{s_{X_1}^2 + s_{X_2}^2}{2}}$$

$$df = 2n - 2$$

\bar{X}_n represents the average of the mean gray values for a single compression condition at the t=0 seconds and t=10 minutes timepoints. Assuming equal variance, the term s_p indicates the pooled variance of both samples populations. The degrees of freedom, or df , are used to calculate the t-statistic which is utilized to assess significance. The term n represents the sample size. A 95% confidence interval was selected to determine the a corresponding p-value from a t-statistic. If the p-value was less than 0.05, the null hypothesis was rejected and compression was assessed to have a significant effect on diffusion into alginate microbeads.

Macrobeads

A similar independent, two-sample t -test that assumed equal variance was performed on the ratios of the radii over which diffusion did not occur to the total radii of the macrobeads to compare the significance of compression on diffusivity. T -tests comparing the effects of compression on the diffusivity of various weight markers into macrobeads were performed for different lengths of incubation periods.

Example t-statistic calculation for testing significance of compressions on diffusion:

$$\begin{aligned} \mathbf{H}_0: & \text{Mean radial diffusion dist. with 10 C} \\ & = \text{Mean radial diffusion dist. with No C} \end{aligned}$$

$$\begin{aligned} \mathbf{H}_A: & \text{Mean radial diffusion dist. with 10 C} \\ & \neq \text{Mean radial diffusion dist. with No C} \end{aligned}$$

$$t = \frac{\text{Mean radial diffusion dist. with 10 C} - \text{Mean radial diffusion dist. with No C}}{\left(\sqrt{\frac{(\text{Variance of 10 C sample})^2 + (\text{Variance of No C sample})^2}{2}} \right) \left(\sqrt{\frac{2}{\# \text{ of samples}}} \right)}$$

$$d.f. = 2 (\# \text{ of samples}) - 2$$

Pilot Testing

Composition Variations

A variety of AA and CL combinations were created in macrobead, microbead, and slab morphologies. Fluorescence imaging was used to evaluate the relative pore size of each composition condition using both FITC weight markers (4 kDa, 70 kDa, and 500 kDa) and polystyrene fluorescent beads (26 nm and 47 nm). Fluorescent testing was general conducted using rapid diffusion tests and 24 hour incubation tests and ImageJ analysis.

Table 4. Alginate and CaCl₂ variations

% AA	% CaCl ₂ Crosslinker		
	0.25%	0.5%	1.5%
0.5%	-----	0.5% AA / 0.5% CL	0.5% AA / 1.5% CL
2%	2% AA / 0.25% CL	2% AA / 0.5% CL	2% AA / 1.5% CL
3%	-----	3% AA / 0.5% CL	3% AA / 1.5% CL

Alginate-Gelatin Mixtures

Alginate-Gelatin mixtures were created in varying ratios in macrobead, microbead, and slab morphologies [32]. Fluorescence imaging was used to determine the relative pore size of each mixture using both FITC weight markers (4 kDa, 70 kDa, and 500 kDa) and polystyrene fluorescent beads (26 nm and 47 nm). Fluorescent testing was general conducted using rapid diffusion tests and 24 hour incubation tests and ImageJ.

Table 5. Alginate-Gelatin Compositions [1.5 % CaCl₂]

% AA	% Gelatin			
	0.5%		1.5%	
0.5%	1:1 0.5% AA / 0.5% Gel	2:1 0.5% AA / 0.5% Gel	1:1 0.5% AA / 1.5% Gel	2:1 0.5% AA / 1.5% Gel
2%	1:1 2% AA / 0.5% Gel	2:1 2% AA / 0.5% Gel	1:1 2% AA / 0.5% Gel	2:1 2% AA / 1.5% Gel

Alginate-CMC Mixtures

Sodium alginate and carboxymethyl cellulose (CMC) were dissolved in 0.9% NaCl at a 3:1 ratio (2% w/v AA, 0.67% w/v CMC). Macrobeads and microbeads were manufactured using aforementioned atomization methods. Fluorescence imaging was used to determine the relative pore size of each mixture using both FITC weight markers (4 kDa, 70 kDa, and 500 kDa) and polystyrene fluorescent beads (26 nm and 47 nm). Fluorescent testing was general conducted using rapid diffusion tests and 24 hour incubation tests and ImageJ.

Mach-1™ Compression

The following alginate compositions, 2% AA / 0.5% CL, 2% AA / 1.5% CL, 0.5% AA / 1.5% CL, and 2% AA / 2% Gel / 1.5% CL, were exposed to Mach-1™ compression to mechanically break crosslinks in the hopes of expanding the average pore size. The alginate constructs underwent compression/relaxation cycles using a ramp release function or a stress relaxation with a consecutive move relative. During these sequences, beads were compressed to 25% of their diameter at a constant rate of 0.5 m/s². The compression was held for 1 or 5 seconds, then released at the same rate. Beads were subjected to five or ten consecutive compressions with a find contact function between each compression. Viscoelastic profiles were then generated and analyzed to characterize material properties.



Figure 7. Illustration of Mach-1™ set-up. Mach-1™ for mechanical compression is connected to a PC and controlled using Mach-1™ Motion software. Samples are loaded onto the Mach-1™ platform and compressed by a transducer. Transducer signals are sent to the PC for data logging and profile plotting.

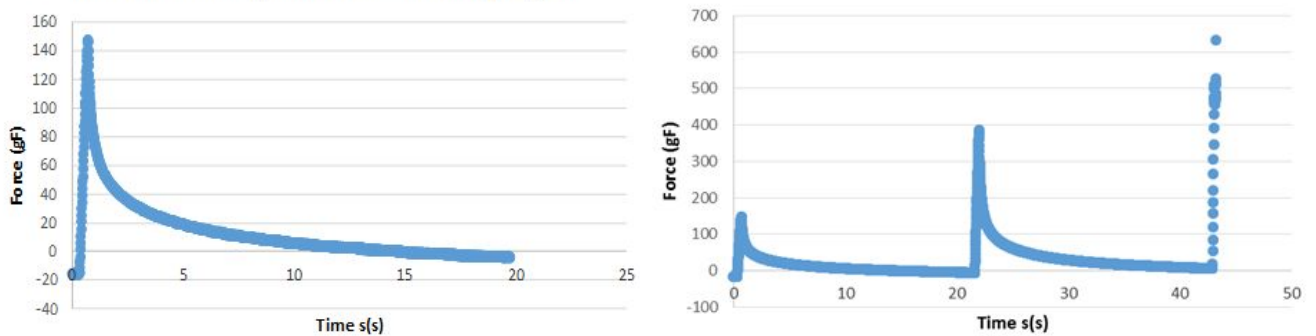


Figure 8. Sample Stress-Relaxation Plots of Crosslinked Alginate using Mach-1™ (from BIOE 140L Winter 2016). The left chart is indicative of a single stress-relaxation cycle. The right chart illustrates multiple rounds of stress-relaxation. Number of cycles will be optimized for each alginate composition so as to minimize structural damage.

Results

Morphology and physical behavior of different alginate constructs

Increased alginate and CaCl₂ concentrations corresponded with increased opacity and physical hardness, as determined by subjective observation. Alginate slabs took approximately three days to manufacture at higher alginate and crosslinker concentrations, but up to 7 days for lower concentrations. Additionally, slabs resulted in inconsistent crosslinking due to variations in drying times. Lower alginate and crosslinker concentrations also resulted in macro and microbeads with inconsistent morphology. Beads manufactured with 0.5% sodium alginate and or 0.5% CaCl₂ were unable to hold a consistent spherical shape, especially under mechanical compression. Atomized microbeads held mostly uniform shape with a diameter between 600 and 700 μm. Some beads were not spherical in shape, so beads that were considered to be uniformly circular were chosen for analysis.

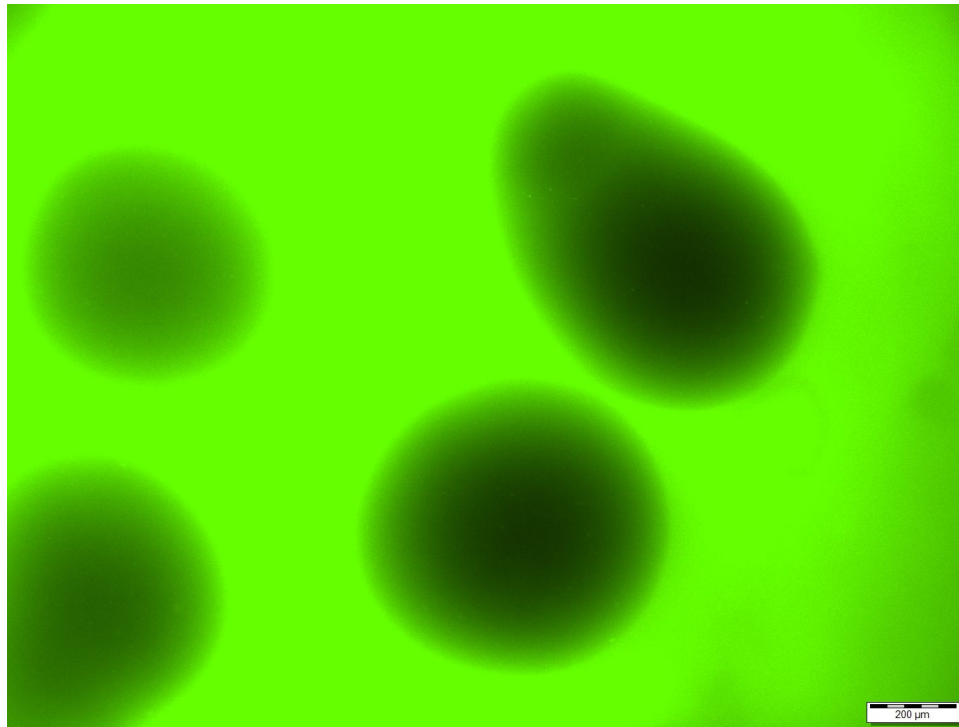


Figure 9. Morphology of Atomized Crosslinked Alginate Microbeads. Alginate microbeads shown are incubated in 500 kDa FITC-dextran. Bead diameter: approximately 600 μm.

Alginate-Gelatin macrobeads dropped into CaCl_2 baths had flattened morphologies on contact, with similar opacity profiles as pure alginate hydrogels. When atomized, alginate-gelatin microbeads did not form individual microspheres, and instead gelled into larger slabs, at the standardized atomization needle height and liquid and gas flowrates. After atomization, individual alginate-gelatin microbeads were unable to be discriminated under phase contrast microscopy. Alginate-CMC macrobeads formed similarly to pure alginate hydrogels, but exhibited a higher observed physical hardness.

Radial Diffusivity Ratios for Macrobeads

Macrobeads (2% AA, 1.5% CaCl_2) were incubated in 4kDa FITC-dextran dye for 60 minutes to allow for diffusion to occur. Radial diffusion distances of the fluorescent dye into the bead interior at 60 minutes were averaged and compared to the baseline fluorescence measured along the bead border at $t=0$. No significant difference in radial diffusion distance of the 4 kDa weight marker was observed after 60 minutes. The effect of mechanical compression on diffusion of the 4 kDa marker into alginate microbeads was tested as well. Macrobeads were compressed five times using a ramp release cycle facilitated by the Mach-1TM instrument. After each compression, a random sample of beads were removed and incubated in fluorescent dye for 60 minutes. For each compression condition, the ratio of the area over which diffusion occurred to the total area of the bead was calculated for multiple beads. These values were compared to the baseline ratios calculated for macrobeads that had experienced no compressions. Mechanical compression of macrobeads were not shown to have a significant effect on diffusion of the 4 kDa weight marker.

Similarly, macrobeads with the same chemical composition were incubated for 60 minutes in 500 kDa FITC-dextran dye. By performing a statistical analysis comparing the mean radial diffusion distances of the fluorescent dye into the bead at $t=0$ and $t=60$ minutes, no significant increase in diffusion was observed over the hour-long incubation

period. As with the 4 kDa marker, the effect of compression on diffusivity of 500 kDa molecules into alginate macrobeads was tested. No significant effect on diffusion was observed for any number of mechanical compressions between one and five successive manipulations.

Alginate macrobeads mechanically compressed between one and five times were additionally incubated in 26 nm and 47 nm polystyrene fluorescent beads separately for 60 minutes. Successive compressions were found to have no significant effect on the distance of diffusion of either weight marker into the macrobead.

Table 6: Confirmed Diffusion of Fluorescent Dyes in Macrobeads and Microbeads, uncompressed and compressed

Alginate Construct	MWCO	Effective Pore Size	Confirmed Diffusion (No Compression)	Confirmed Diffusion (w/ 5 Compressions)	P-Value
Macrobeads 2% AA, 1.5% CaCl ₂	4 kDa	2 nm	No	No	0.82
	70 kDa	6 nm	No	No	N/A [*]
	500 kDa	11 nm	No	No	0.63
	6,400 kDa	26 nm	No	No	0.71
	38,000 kDa	47 nm	No	No	0.85
Microbeads 2% AA, 1.5% CaCl ₂	4 kDa	2 nm	Yes	Yes	N/A [^]
	70 kDa	6 nm	Yes	Yes	N/A [^]
	500 kDa	11 nm	No	Plausible	0.72
	6,400 kDa	26 nm	No	Inconclusive	0.51
	38,000 kDa	47 nm	No	No	0.89

^{*}Insufficient data

[^]Confirmed diffusion based on literature review [31]

ImageJ Analysis of Microbeads

Images of microbeads (2% AA, 1.5% CaCl₂) incubated in all fluorescent dyes were compared at t = 0 minutes and t = 10 minutes, with gray value profiles generated and compared for each condition at these two timepoints. For all dye conditions at t = 0 minutes, all gray value profiles featured indentations that represent the bead interior.

For beads incubated in the 70 kDa FITC-dextran, these indentations became shallower over a 10 minute period, and the gray values within the bead approached the background gray value. There was no discernable difference in the gray value plot behavior between uncompressed microbeads and the 5C and 10C microbeads incubated in 70 kDa FITC-dextran. Similarly, there was no discernable difference in the gray value plot behavior between microbeads incubated in 4 kDa FITC-dextran and microbeads incubated in 70 kDa FITC-dextran.

For microbeads incubated in 500 kDa FITC-dextran, gray value plot behavior varied between uncompressed and compressed bead conditions. At both 0C and 5C, the gray value indentations did not increase appreciably relative to the background values. At 10C, the gray values in the region within the microbead appeared to increase relative to background values. Similar behavior was documented for microbeads incubated in 26 nm PS, with a slight increase in gray value plots for all conditions, but no significant change occurred with more compressions.

Microbeads incubated in 47 nm PS had no significant change in gray value plot from time t = 0 minutes to t = 10 minutes.

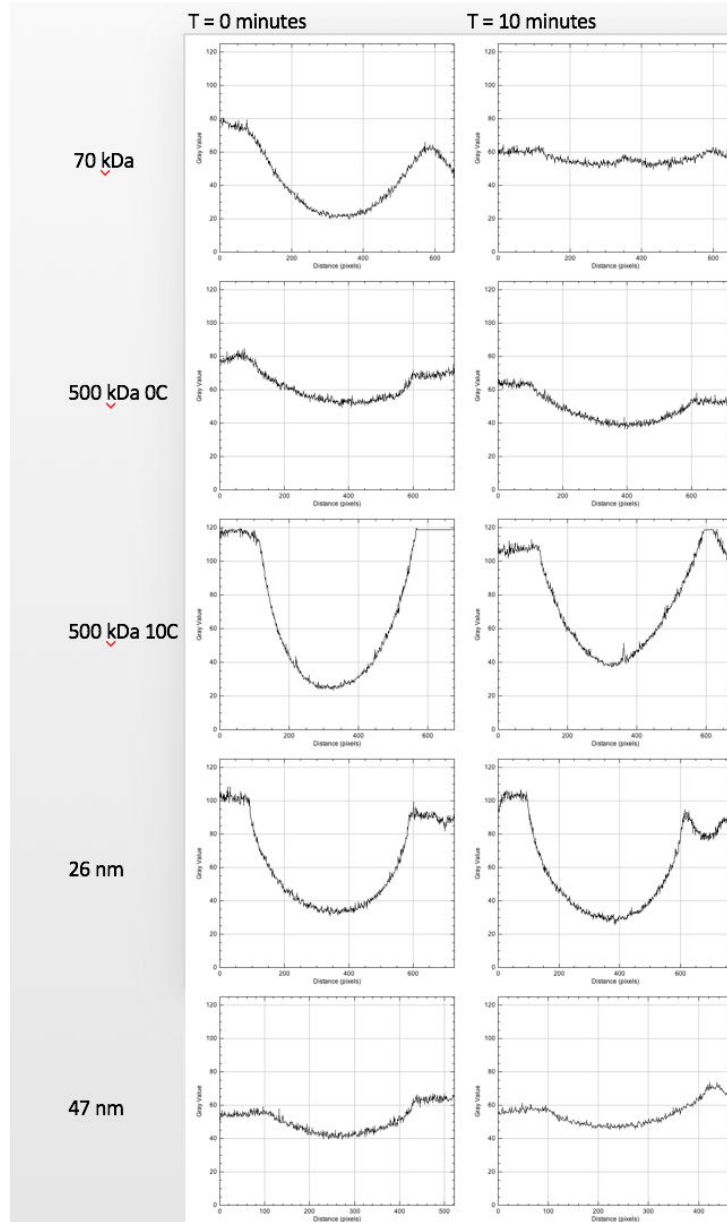


Figure 10. Gray value plots across alginate microbead diameter. Plots were generated using ImageJ for images taken at 60 second intervals. High gray values correspond to high fluorescent intensity, while low gray values correspond with low fluorescent intensity.

Mean gray values for a single microbead were calculated for each molecular weight marker at t=0 and t=10 minutes following incubation. If diffusion of the weight marker into the microbead were to occur, the mean gray value over the cross-sectional area of the bead would be expected to increase over the 10 minute incubation period. In the

500 kDa condition, the mean gray value decreased after 10 minutes in microbeads exposed to 0, 5, and 10 compressions. However, following statistical analysis no significant difference in gray values, and subsequently no inward diffusion of the weight marker, was observed in any of the three compression conditions. Similarly, no statistically significant difference in diffusion of the 26 nm and 47 nm weight markers over the incubation period were observed at either 0, 5, or 10 compressions.

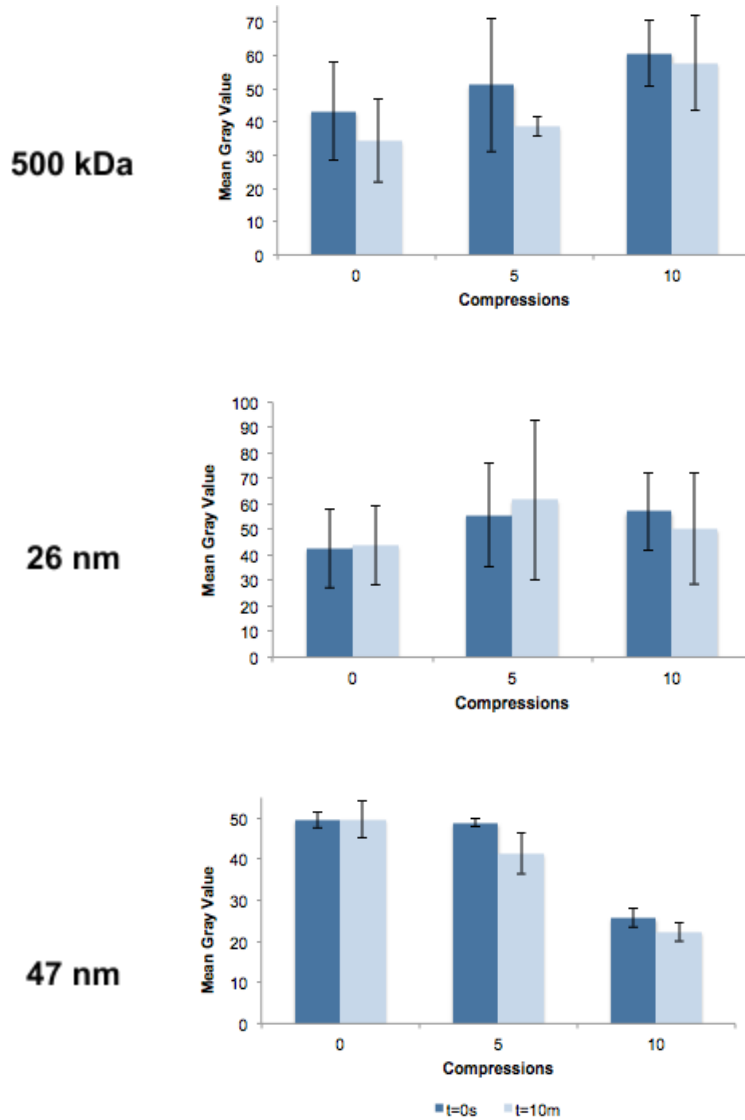


Figure 11. Change in mean gray value of cross-sectional area of alginate microbeads incubated in various fluorescent weight markers. ImageJ was used to evaluate gray values over specific bead areas. No significant differences in gray values over 10 minute weight marker incubation were observed for any compression condition. Error bars represent standard deviation from the mean.

Diffusion Modeling of Microbead Constructs

Based on the results of the observed microbead incubation in fluorescent dyes, COMSOL models were generated, given what was observed in the incubation experiments. Simple 2D models were generated with Dirichlet boundary conditions set to match what was observed using the fluorescent microscope. Diffusivities of the bead interior were determined using a parametric sweep and subjectively chosen to match what was experimentally observed.

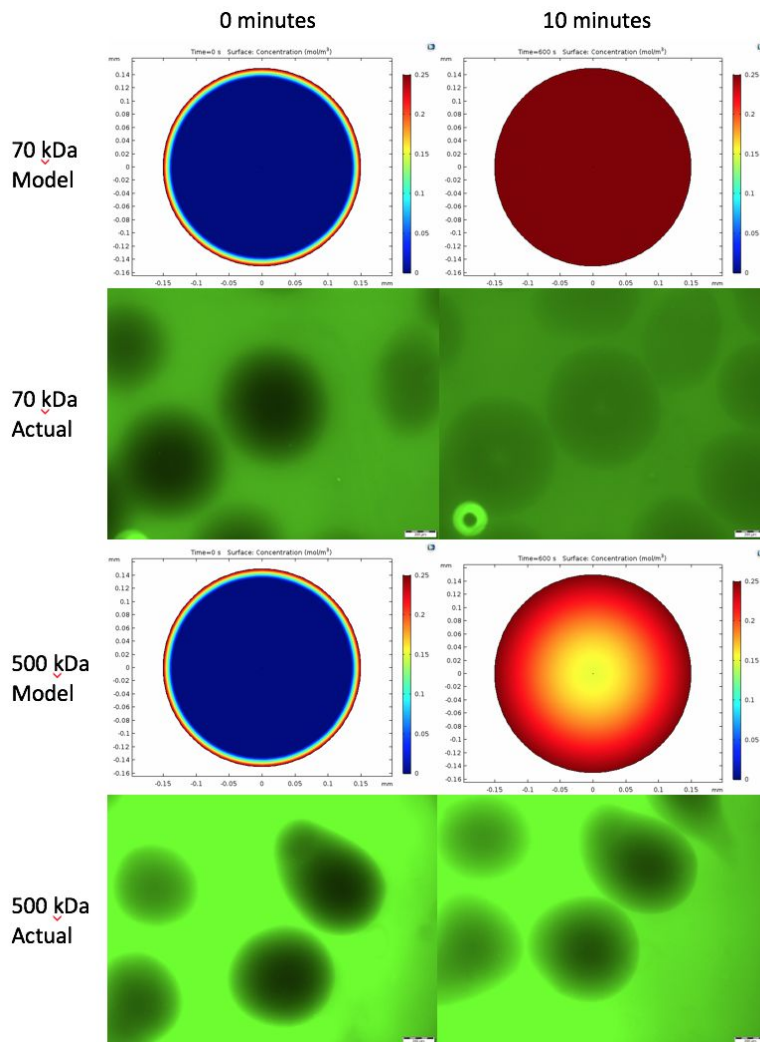


Figure 12. COMSOL modeling of microbead diffusivities. Diffusion of FITC-dextran was modeled using the "Transport of Diluted Species" module. Diffusivity values were chosen based on trial and error to match what was observed using fluorescent microscopy. Concentration gradients shown in the COMSOL models are represented by the indicated color gradient. COMSOL models for 70 kDa FITC dextran and 500 kDa FITC-dextran were generated for conditions in which inward diffusion occurred: 0C 70 kDa and 10C 500 kDa.

Table 7. Estimated Microbead Diffusivities based on COMSOL modeling

Condition	Estimated Diffusivity
0C/5C/10C, 70 kDa	$4.0 \times 10^{-11} \text{ m}^2/\text{s}$
10C, 500 kDa	$9.0 \times 10^{-12} \text{ m}^2/\text{s}$

Based on these simplified models, 1D profile plots of concentration over the diameter of the bead were generated. These plots were similar in behavior to the gray value plots obtained using ImageJ, where areas of lower fluorescent intensity or concentration is the least at the center of the microbead.

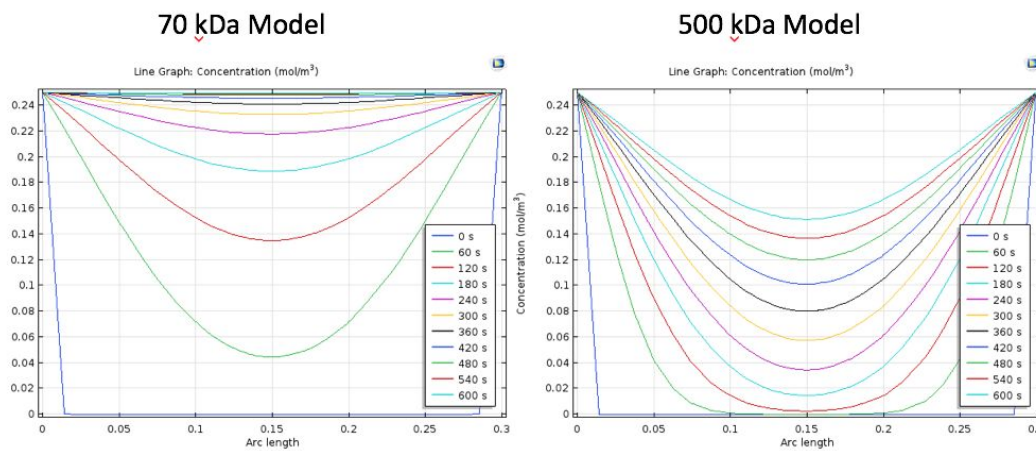


Figure 13: 1D Concentration Profile Plots for 70 kDa and 500 kDa Microbead Models. Concentration was plotted along the arc length of the diameter of a simulated microbead. Curves were drawn at 60 second intervals of the simulation.

Viscoelastic Profiles for Macrobead Compressions

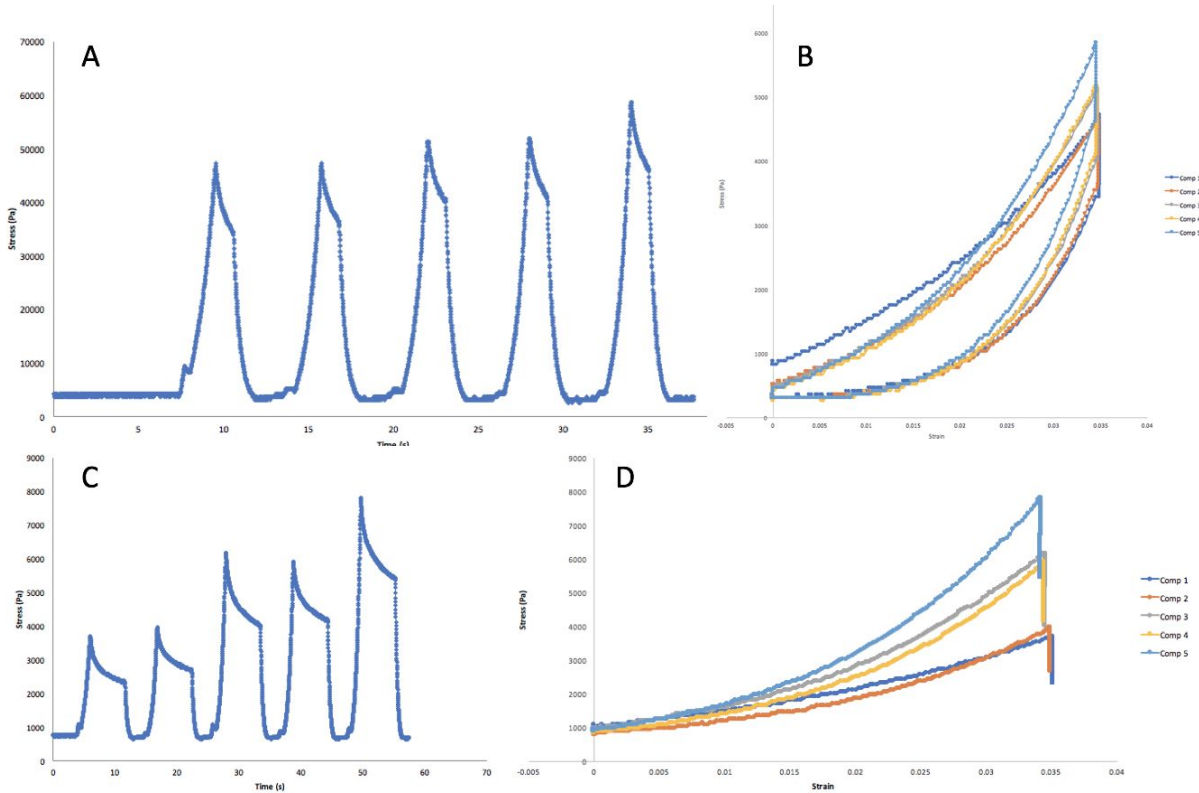


Figure 14. Recovery Time Graphs and Viscoelastic Profiles of Compressed Alginate Macrobeads. Viscoelastic profiles were generated using data collected during Mach-1™ compressions. The Mach-1™ device recorded time (s), position (m), and force (gf). Force (N), stress, and strain (Pa) were calculated. A) Stress versus time graph for 2% AA / 1.5% CL beads subjected to five 1 s ramp release mechanism. B) Stress versus strain graph for 2% AA / 1.5% CL beads subjected to five 1 s ramp release mechanism. C) Stress versus time graph for 2% AA / 1.5% CL beads subjected to five five second long stress relaxation mechanism followed by a move relative function. D) Stress versus strain graph for 2%AA / 1.5% CL beads subjected to five five second long stress relaxation mechanism followed by a move relative function.

Table 8. Material Properties of Compressed Alginate Microbeads

Number of Compressions	$E_{\text{Stress Relaxation}}$ (kPa)	$E_{\text{Ramp Release}}$ (kPa)	Δt (s)
1	76.05	110.40	2.59
2	89.86	120.70	2.60
3	150.56	135.30	2.64
4	146.48	139.76	2.54
5	200.66	157.60	2.63

Discussion

Pilot testing revealed that several composition manipulations were unviable for eventual experimentation. Alginate-gelatin mixtures were not examined due to inconsistent shape and microbead gelation. Similarly, low alginate and crosslinker conditions yielded inconsistent morphologies that were deemed unsuitable for investigation. High alginate and crosslinker conditions, despite their consistent morphology, were also excluded from investigation after pilot testing revealed restricted diffusivity at weight marker sizes larger than 70 kDa. As a result, analysis and process optimization focused on macrobeads and microbeads consisting of 2% AA, 1.5% CL, crosslinked for 30 minutes (macrobeads) and 60 minutes (microbeads). This formulation was the most ideal for manipulation and imaging purposes, as constructs fabricated under these conditions yielded the most uniform and manipulable beads. Alginate slabs were not considered for analysis due to the increased time of manufacturing, limited by drying time, which was deemed to be impractical for diffusivity analysis.

ImageJ analysis of microbead diffusivities indicated that the molecular weight cutoff of 2% AA, 1.5% CL microbeads is 70 kDa uncompressed, and 500 kDa compressed 10 times, indicating that the pore size of these constructs is less than 6 nm and 11 nm, respectively. For most 500 kDa FITC-dextran incubations, relative increases in gray value within a microbead were not easily discriminated. After 10 compressions, the gray value change after 10 minutes of incubation in the 500 kDa FITC-dextran became more pronounced, suggesting an increase in the diffusivity of the microbead. Increases in the diffusivity can be interpreted as an increase in the pore size of the alginate microbead. Because the dye was able to penetrate further into the microbead after compressions it is implied that the Stokes radius of the dye is less than the pore size at the membrane. Therefore, the pore size of the alginate microbead must be greater than the 500 kDa FITC-dextran after 10 compressions.

However, the gray value plots for the 500 kDa, 10C condition do not agree with COMSOL modeling of the concentration change. COMSOL models suggest that after 10 minutes of incubation, the concentration of dye at the center of the bead is greater than half of the background concentration. In comparison, gray value plots obtained using ImageJ indicate that the amount of inward diffusion is not as great despite the visual agreement between the model and the observed results. In order to reconcile the differences between the simplified model generated in COMSOL and the images captured using fluorescence microscopy, the generation of a calibration curve is necessary. However, despite controls taken to minimize photobleaching, the generation of a calibration curve to translate fluorescence to concentration was inconsistent. Lower concentrations were difficult to obtain analogous gray values due to rapid photobleaching. In addition, variation in real time incubation changed the relative background fluorescence in each experiment, which may or may not correspond to varying concentrations. As a result, optimization of the microbead incubation method is necessary in order to mitigate the photobleaching of the fluorescent dye.

Viscoelastic profiling assumed perfectly elastic behavior in order to determine approximate Young's modulus values over multiple compressions. Due to the viscoelastic character of sodium alginate hydrogels, further analysis is needed to determine precise values. Approximate values, however, suggest that the alginate constructs experience strain hardening with consecutive compressions. This is seen through the general increase in the Young's modulus over the course of testing, indicating that the construct is not weakening. Taking into account ImageJ analysis of microbead diffusivities, despite the strain hardening of the alginate constructs, 10 ramp-release compressions appear to increase the molecular weight cutoff of these alginate constructs to ≥ 500 kDa. However, due to time constraints and incomplete optimization of compression data collection, viscoelastic profiles for 10C microbeads were not obtained. As a result, it is unknown whether strain hardening continued to occur beyond 5 compressions, or if strain softening occurred post 5C. Strain softening would correspond to the weakening of the bead and potential damage to the construct. If a bead were to be damaged, microcracks on the surface of the microbead may influence the molecular weight cutoff of the hydrogel, therefore skewing our dataset. Further testing needs to be conducted to determine the exact effects of mechanical manipulation on the molecular weight cutoff and, therefore, pore size of alginate hydrogels. In addition, visual confirmation of bead topography post-compression is necessary to determine whether compressions induce damage.

Future Directions

Throughout experimentation, it was determined that the 60 minute incubation period for macrobeads did not allow for adequate diffusion time in relation to the radial distances of the beads. Therefore, in future experiments, longitudinal diffusion studies, or experiments with incubation periods spanning up to four days, should be conducted to observe diffusion behavior over longer periods of time.

In addition, several directions need to be explored in terms of mechanical compressions and material characterization. Viscoelastic data needs to be analyzed using complex moduli for more representative material characterization. Additionally, the number of consecutive compressions should be increased in order to determine the ultimate tensile strength of the given alginate constructs. Further research into varying compression time and distance must also be conducted to determine effects on overall porosity.

Additional manipulations may lead to the increase in pore size of alginate hydrogels. Sodium citrate is a compound that reverses crosslinking in alginate based hydrogels. Whether or not this has an appreciable effect on the pore size of alginate based hydrogels has yet to be determined. Future studies may look into the optimization of citrating alginate based hydrogels to tune pore size. Similarly, future work may look into the effects of lyophilization on pore size. Lyophilization has been previously used to influence the microporosity of alginate based hydrogels [2], so studies may be conducted to determine how nanoporosity can be influenced by different lyophilization profiles.

Summary and Conclusion

Our project sought out to determine methods to increase the pore size of alginate based hydrogels in order to expand its applications in the biomedical field. The primary manipulations we analyzed were hydrogel composition, fabrication method, and mechanical compressions, and we examined each manipulations' effect on the effective pore size of the resultant hydrogel construct. For the optimal hydrogel formulation (2% AA, 1.5% CL), we found that mechanical compressions had a nonsignificant effect on macrobead diffusivity. However, it may have had a significant effect on microbead diffusivity. Future work still needs to be completed to determine exactly how mechanical compressions affects bead integrity, and the intrinsic material properties of alginate-based hydrogels. In addition, further test method optimization is necessary to create comprehensive diffusion models to relate what is observed using fluorescent microscopy methods to precise mathematical constants, to which pore size can be related. While the desired goal of increasing the pore size to the 10-30 nm range was not reached, we have set a foundation for future groups to continue exploring methods to tune the porosity of alginate based hydrogels.

Engineering Standards and Realistic Constraints

Manufacturability

The objectives of this project demand manipulation of natural properties of a naturally-occurring material for primary use in biomedical applications. As such, maintaining consistency when producing alginate hydrogel microcapsules with desired pore sizes is essential to ensure replicable results in downstream applications of this method. Method development should yield protocols that reliably produce alginate hydrogel constructs with the target pore size throughout the batch. Additionally, if uniformity of pore size is not achieved within a single microcapsule, calculated diffusion rates will be meaningless, thereby eliminating controlled drug delivery applications.

Economic

Considering the relative ease to produce alginate hydrogels, the methods developed by this project should preserve the simplicity of existing protocols. Having simple protocols that do not require specialized equipment (i.e. UV light sources for photocrosslinking, lyophilizers) or expensive reagents can allow more people to perform the techniques at reasonable costs. The majority of the economic cost of the project is borne by the fluorescent weight markers that will act as indicators of standard pore size achievement. Once standard protocols are established, the production of alginate microcapsules with manipulable pore size will be relatively low-cost and straight forward.

Sustainability

Experimental methods should not generate waste or harmful byproducts or require energy-intensive equipment. The devised setup for alginate microcapsule formation primarily utilizes compressed air to produce uniform, replicable samples - a method with no toxic by-products and minimal energy expenditure. Mechanical compression to induce broken crosslinks and subsequent increases in pore sizes using a Mach-1 system generates no additional waste.

Health & Safety

Proposed methods of alginate microcapsules carry minimal health and safety risks to both manufacturer and customer. Minimal training in regard to handling compressed air tanks, however, is required for capsule formation pursuant to the atomization setup in use. Because alginate is a biocompatible material, it presents no biological risk and even has a number of potential *in vivo* applications. Other *in vitro* applications involving alginate microcapsules with modifiable pore sizes could actually promote global human health by acting as non-cytotoxic cell viability assays for experiment drugs or biomolecular therapies.

Ethical

Accommodating wider ranges of alginate hydrogel pore sizes enable toolkit development for a variety of biomedical applications. Such applications could promote human health, such as target drug delivery, or allow for easier and faster evaluation of biomolecular therapies or interventions, such as cytotoxicity testing. By enabling a cheaper, more efficient testing mechanism to aid in the development of therapies or pharmaceuticals, the project demonstrates its ethical value to not only the biomedical field, but to society as a whole.

Bibliography

- [1] Simpliciano, Cheryl, Larissa Clark, Behrokh Asi, Nathan Chu, Maria Mercado, Steven Diaz, Michel Goedert, and Maryam Mobed-Miremadi. "Cross-linked alginate film pore size determination using atomic force microscopy and validation using diffusivity determinations." *Journal of Surface Engineered Materials and Advanced Technology* 3, no. 04 (2013): 1.
- [2] Annabi, N., Nichol, J. W., Zhong, X., Ji, C., Koshy, S., Khademhosseini, A., & Dehghani, F. (2010). Controlling the Porosity and Microarchitecture of Hydrogels for Tissue Engineering. *Tissue Engineering. Part B, Reviews*, 16(4), 371–383. <http://doi.org/10.1089/ten.teb.2009.0639>
- [3] Patil, M., Mehta, D. S., & Guvva, S. (2008). Future impact of nanotechnology on medicine and dentistry. *Journal of Indian society of periodontology*, 12(2), 34.
- [4] Gao, W., Zhang, Y., Zhang, Q., & Zhang, L. (2016). Nanoparticle-hydrogel: a hybrid biomaterial system for localized drug delivery. *Annals of biomedical engineering*, 44(6), 2049-2061.
- [5] Lee, K. Y., & Mooney, D. J. (2012). Alginate: properties and biomedical applications. *Progress in Polymer Science*, 37(1), 106–126. <http://doi.org/10.1016/j.progpolymsci.2011.06.003>
- [6] Poveda-Reyes, S., Moulisova, V., Sanmartín-Masiá, E., Quintanilla-Sierra, L., Salmerón-Sánchez, M. and Ferrer, G. G. (2016), Gelatin—Hyaluronic Acid Hydrogels with Tuned Stiffness to Counterbalance Cellular Forces and Promote Cell Differentiation. *Macromol. Biosci.*, 16: 1311–1324. doi:10.1002/mabi.201500469
- [7] Langer, R. (2000). Biomaterials in drug delivery and tissue engineering: one laboratory's experience. *Accounts of Chemical Research*, 33(2), 94-101.
- [8] Erickson, H. P. (2009). Size and shape of protein molecules at the nanometer level determined by sedimentation, gel filtration, and electron microscopy. *Biological procedures online*, 11(1), 32.
- [9] Park, S. N., Park, J. C., Kim, H. O., Song, M. J., & Suh, H. (2002). Characterization of porous collagen/hyaluronic acid scaffold modified by 1-ethyl-3-(3-dimethylaminopropyl) carbodiimide cross-linking. *Biomaterials*, 23(4), 1205-1212.
- [10] Dolega, M. E., Delarue, M., Ingremeau, F., Prost, J., Delon, A., & Cappello, G. (2017). Cell-like pressure sensors reveal increase of mechanical stress towards the core of multicellular spheroids under compression. *Nature Communications*, 8, 14056.

- [11] Valade, D., Wong, L. K., Jeon, Y., Jia, Z. and Monteiro, M. J. (2013), Polyacrylamide hydrogel membranes with controlled pore sizes. *J. Polym. Sci. A Polym. Chem.*, 51: 129–138. doi:10.1002/pola.26311
- [12] Mobed-Miremadi, M. (2014). High-Throughput Methods for Miniaturization of Implantable Artificial Cells. In *Selected Topics in Nanomedicine* (pp. 411-427).
- [13] Szymanski, J. M., & Feinberg, A. W. (2013). Fabrication of freestanding alginate microfibers and microstructures for tissue engineering applications. *Biofabrication*, 6(2), 024104.
- [14] Vegas, A. J., Veisoh, O., Gürtler, M., Millman, J. R., Pagliuca, F. W., Bader, A. R., ... & Tam, H. H. (2016). Long-term glycemic control using polymer-encapsulated human stem cell-derived beta cells in immune-competent mice. *Nature medicine*, 22(3), 306-311.
- [15] Risa, E. L., Kolar Venkat, S., Antell, B., & Mobed-Miremadi, M. (2017). Modeling the Combined Effect of Convection and Diffusion in Cross-linked Alginate Capsules.
- [16] Kolar Venkat, S., Risa, E. L., Antell, B., & Mobed-Miremadi, M. (2017). Effect of Multiple Confined Compression/Stress Relaxation Cycles on Cross-linked Alginate Pore Size.
- [17] Merino, S., Martín, C., Kostarelos, K., Prato, M., & Vázquez, E. (2015). Nanocomposite hydrogels: 3D polymer–nanoparticle synergies for on-demand drug delivery. *ACS nano*, 9(5), 4686-4697.
- [18] Rohringer, S. (2017, July 2). PLA vs ABS: Filaments for 3D Printing Explained & Compared. Retrieved December 05, 2017, from <https://all3dp.com/pla-abs-3d-printer-filaments-compared/>
- [19] Wayne, J. S., McDowell, C. L., Shields, K. J., & Tuan, R. S. (2005). In vivo response of polylactic acid–alginate scaffolds and bone marrow-derived cells for cartilage tissue engineering. *Tissue engineering*, 11(5-6), 953-963.
- [20] Ultimaker 3 | Ultimaker. (n.d.). Retrieved December 05, 2017, from <https://ultimaker.com/en/products/ultimaker-3>
- [21] Szekalska, M., Puciłowska, A., Szymańska, E., Ciosek, P., & Winnicka, K. (2016). Alginate: Current Use and Future Perspectives in Pharmaceutical and Biomedical Applications. *International Journal of Polymer Science*, 2016. <https://www.hindawi.com/journals/ijps/2016/7697031/>

- [22] Miranda, J. P., Rodrigues, A., Tostoes, R. M., Leite, S., Zimmerman, H., Carrondo, M. J., & Alves, P. M. (2010). Extending hepatocyte functionality for drug-testing applications using high-viscosity alginate-encapsulated three-dimensional cultures in bioreactors. *Tissue Engineering Part C: Methods*, 16(6), 1223-1232.
<https://www.ncbi.nlm.nih.gov/pubmed/20184401>
- [23] Jeon, O., Bouhadir, K. H., Mansour, J. M., & Alsberg, E. (2009). Photocrosslinked alginate hydrogels with tunable biodegradation rates and mechanical properties. *Biomaterials*, 30(14), 2724-2734.
- [24] Seow, W. Y. *et al.* Transparent crosslinked ultrashort peptide hydrogel dressing with high shape-fidelity accelerates healing of full-thickness excision wounds. *Sci. Rep.* 6, 32670
- [25] Lucinda-Silva R.M., Evangelista M.C. (2003). Microspheres of alginate-chitosan containing isoziadin. *J. Microencapsul.* 20:145–152.
- [26] Acarturk F., Takka S. (1999). Calcium alginate microparticles for oral administration: II. Effect of formulation factors on drug release and drug entrapment efficiency. *J. Microencapsul*, 16, 291–301.
- [27] Straccia, M.C.; d'Ayala, G.G.; Romano, I.; Oliva, A.; Laurienzo, P. (2015) Alginate Hydrogels Coated with Chitosan for Wound Dressing. *Drugs*, 13, 2890-2908
- [28] Zhao, K., Di, Q., Cao, X., Wang, M., Deng, L., & Wang, F. (2016). Production of Biodiesel Using Immobilized Lipase and the Characterization of Different Co-Immobilizing Agents and Immobilization Methods. *Sustainability*, 8(9), 764.
- [29] Khani, Z., Jolivalt, C., Cretin, M., Tingry, S., & Innocent, C. (2006). Alginate/carbon composite beads for laccase and glucose oxidase encapsulation: application in biofuel cell technology. *Biotechnology letters*, 28(22), 1779-1786.
- [30] Tow, E. W. (2017). Organic fouling of desalination membranes. (Doctoral dissertation, Massachusetts Institute of Technology).
- [31] Mobed-Miremadi, M., Asi, B., Parasseril, J., Wong, E., Tat, M., & Shan, Y. (2013). Comparative diffusivity measurements for alginate-based atomized and inkjet-bioprinted artificial cells using fluorescence microscopy. *Artificial cells, nanomedicine, and biotechnology*, 41(3), 196-201.
- [32] Li, X. Y., Chen, X. G., Liu, C. S., Liu, C. G., & Xue, Y. P. (2008). Preparation of alginate-gelatin capsules and its properties. *Frontiers of Materials Science in China*, 2(3), 253-260.

[33] International Medical Devices Expo (IMD 2009) and Advanced Laser Applications Conference (ALAC 2009). (n.d.). Advanced Laser Applications Conference.

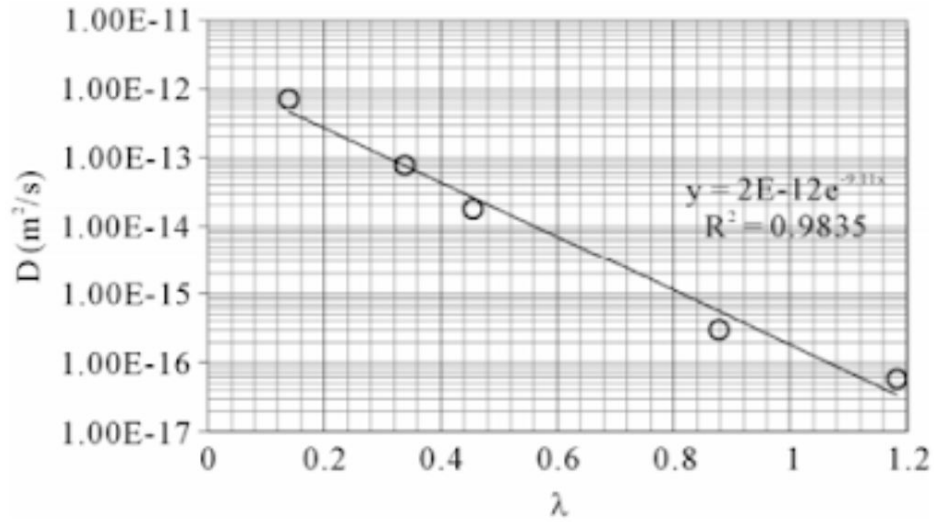
Appendices

Appendix 1. Supplemental Figures and Tables

Appendix 1.1. Estimated Budget for Project

Item	Preliminary Cost
Reagents	
Alginate	\$180
Crosslinking agents	\$145
Chemical modifiers	\$95
Size markers	\$610
Equipment	
Flowmeter + Needles	\$1,140
Mach-1	-
Imaging equipment	-
Total	\$2,170

Appendix 1.2. Membrane diffusivity as a function of solute to membrane pore size [1]



Appendix 1.3. Summary of atomization parameters, bead sizes and dimensionless numbers [33]

F_L (ml/min)	F_A (L/min)	SMD (μ m)	Re	We	Oh
0.5	1.9	1125	0.068	164258	5937
0.5	2.5	800	0.068	298023	7997
0.5	3.0	630	0.068	417786	9468
0.75	1.9	775	0.102	164258	3958
0.75	2.5	700	0.102	309092	5429
0.75	3.0	510	0.102	417786	6312
1.0	1.9	1350	0.137	164258	2968
1.0	2.5	1000	0.137	309092	4072
1.0	3.0	350	0.137	417786	4734

$$Oh = \frac{\sqrt{We}}{Re} = \frac{\mu}{\sqrt{\rho \sigma l}}$$

Appendix 1.4. Effect of AFM scan area on apparent pore size [1]

Sample	CaCl ₂ % (w/v)	Coating	Pore Size Range (nm) at 0.5 μm ²	Pore Size Range (nm) at 0.25 μm ²	Pore Size Range (nm) at 0.15 μm ²	Average Pore Size (nm) at 0.1 μm ²
Alginate MV 0.5% (w/v)	1.5	N/A	11 - 23	7.0 - 16	5.0 - 11	8.4 ± 3.0
Alginate MV 1.0% (w/v)	1.5	N/A	26 - 44	9.0 - 16	7.0 - 15	4.5 ± 1.1
Alginate MV 1.5% (w/v)	1.5	N/A	13 - 35	12 - 28	6.0 - 10	5.2 ± 0.9
Alginate LV 0.5% (w/v)	20	N/A	6.0 - 19	6.0 - 12	4.0 - 18	7.2 ± 2.9
Alginate LV 0.5% (w/v)	20	Chitosan	17 - 24	7.0 - 19	5.0 - 11	7.0 ± 3.1
Dialysis Tubing	N/A	N/A	6.0 - 25	6.0 - 14	5.0 - 13	4.9 ± 3.0

Appendix 1.5. Probability densities of macrobead metrics. Data was analyzed for normality and processed using the Gaussian probability density function. A) 4 kDa FITC-dextran; B) 70 kDa FITC-dextran; C) 26 nm polystyrene; D) 47 nm polystyrene

